Flow in an impeller stirred tank using an immersed boundary method

By R. Verzicco†, G. Iaccarino, M. Fatica AND P. Orlandi‡

1. Motivation and objectives

The present study is concerned with the flow induced by an impeller in a cylindrical tank. Although this is a model problem, it is relevant to many chemical and food-industry technological processes. In the last decade significant effort has been devoted to simulate and predict such flows since full-scale testing is very expensive and considerable savings could be achieved if reliable numerical models could predict the performance of prototypes.

Despite the relatively simple geometries and the low Reynolds numbers involved, the simulation of these turbulent flows is considerably challenging. Some of the difficulties encountered are the strongly inhomogeneous nature of the turbulence, the small surface of the impeller blades, and the large disparity in time and length of flow scales. In particular, given the short blade lengths, the boundary layers developing on their surfaces will not be fully developed; therefore, all turbulence models based on wall functions would give inaccurate results. In addition, RANS models, even when implemented in the unsteady form, are unlikely to capture all of the time scales ranging from that of the vortex shedding at the blade tips to the large scale meridional circulation induced in the tank.

DNS and LES approaches, in contrast, do not suffer from the abovementioned problems although they are more computationally expensive, especially when applied to complex geometry flows. However, in a recent paper by Verzicco *et al.*, (2000), it has been shown that the combination of the "immersed boundary" (IB) procedure with DNS and LES simulations can efficiently be used for the accurate prediction and analysis of many technologically relevant flows. In particular, since the presence of complex boundaries is mimicked by body forces, the simulations are, in fact, carried out on "simple grids", thus taking advantage of the efficiency and accuracy of optimized solution procedures. IB/DNS simulations of complex-geometry turbulent-flows can be carried out with 1-2 million gridpoints on a PC with CPU times ranging between a few hours and a few days.

In this paper we will show some examples of these simulations for an impeller-stirred cylindrical tank, and the results will be compared with experiments and RANS simulations.

2. Physical problem and numerical set-up

The flow investigated in this study is intended to reproduce one of the experiments by Dong *et al.*, (1994). It consists of a cylindrical unbaffled tank stirred by an impeller rotating at constant velocity Ω at mid-height of the tank. The impeller has 8 blades equispaced over the whole azimuthal span. A sketch of the device is given in Fig. 1 where all the lengths have been scaled with the blade radius, which is $R = 1.25$cm. The

† DIMeG, Politecnico di Bari, Via Re David, 200, 70125, Bari, Italy.
‡ DMA, Università di Roma, "La Sapienza", Via Eudossiana, 18, 00184, Roma, Italy

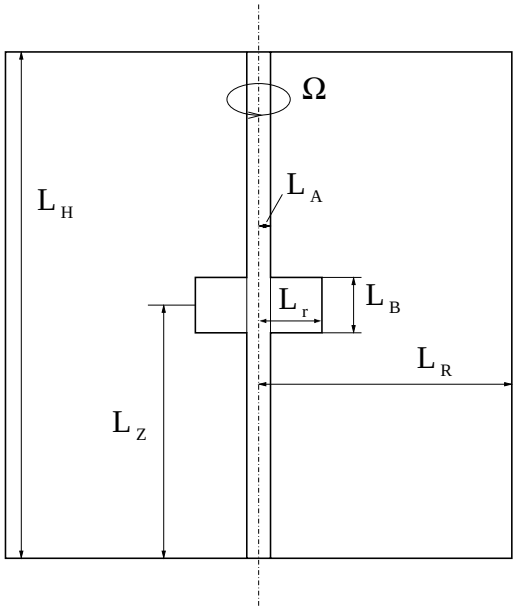

FIGURE 1. Sketch of the mixer geometry: $L_r = 1$, $L_B = 0.8$, $L_A = 0.32$, $L_R = 4$, $L_Z = 4$ and $L_H = 8$.

impeller rotation speed is $\Omega = 100$rpm, and the working fluid is water ($\nu = 10^{-6}\mathrm{m}^2/\mathrm{s}$), thus yielding a Reynolds number $Re = \Omega R^2/\nu = 1636$.

For the numerical solution of the flow, the Navier-Stokes equations are solved in a frame of reference fixed with the impeller and therefore rotating with constant angular velocity Ω. When scaled with the velocity $U = \Omega R$ and the length $L = R$, the equations in the rotating frame read:

$$\frac{D\mathbf{u}}{Dt} = -\nabla p - \frac{1}{Ro}\hat{\Omega} \times \mathbf{u} + \frac{1}{Re}\nabla^2\mathbf{u} + \mathbf{f}, \qquad \nabla \cdot \mathbf{u} = 0, \tag{2.1}$$

with $Ro = 1/2$, $\hat{\Omega}$ the unit vector directed as the impeller rotation vector, and $\mathbf{f}$ a body force to be described later. In this frame of reference the lateral cylindrical wall of the tank has an azimuthal velocity $V_\theta(L_R) = -\Omega L_R$ while the lower horizontal no-slip surface moves according to $V_\theta(r) = -\Omega r$ with r the radial coordinate.

The computational domain is discretized by a mesh which is nonuniform in the radial and axial directions in such a way as to cluster the gridpoints in the blade region and close to the no-slip surfaces (Fig. 2). The mesh is uniform in the azimuthal direction.

An important aspect of this study was the initialization of the simulation. In the experiments, in fact, it has been observed that starting from rest, the flow needs from 5 to 10 minutes to attain a statistically stationary configuration which corresponds to 500 to 1000 impeller revolutions. In the present DNS simulation each revolution is discretized by about 300 time steps, thus requiring $3 \cdot 10^5$ time steps for the initial transient to be exhausted. This computational overhead is clearly unacceptable since it would require, on the finest grid, more CPU hours than the useful part of the simulation. Several strategies have been followed in order to reduce the computation of the transient, and they were only partially successful. The most straightforward approach consisted of several simulations starting from a very coarse grid with a progressive refinement via succes-

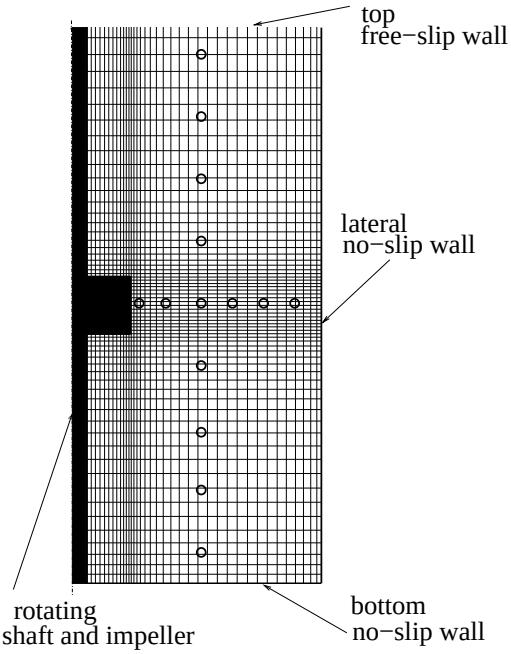

FIGURE 2. Example of grid in a meridional plane and boundary conditions (only one every 6 grid-points are shown). Open circles indicate the position of numerical probes used for the flow analysis.

sive interpolations. The initial flow evolution was obtained by simulating only $1/8^{\text{th}}$ of azimuthal domain and, therefore, only one impeller blade; the field was then replicated in such a way to reproduce the whole impeller. Unfortunately, the adjustments of the solutions from one grid to another introduced additional transients that turned out to be also time consuming. As an alternative we tried to start from a low-Reynolds coarse-grid flow and to increase grid and Reynolds number together. However, in this case the flow adjustment was very slow as well, and almost a total of 500 impeller revolutions were necessary to attain a developed flow field. Most of the transient, however, was simulated over coarse grids; therefore, the total CPU time was equivalent to 40 impeller revolutions on the finest grid.

The boundary body force $\mathbf{f}$ of Eq. (2.1) is prescribed at each time step to establish the desired velocity $\mathbf{V}_b$ on an arbitrary surface that need not coincide with the grid. The time-discretized version of Eq. (2.1a) can be written as,

$$\mathbf{u}^{n+1} - \mathbf{u}^n = \Delta t(RHS + \mathbf{f}) \ , \tag{2.2}$$

where Δt is the computational time step, RHS contains the nonlinear, pressure, and viscous terms, and the superscript denotes the time-step level. To impose $\mathbf{u}^{n+1} = \mathbf{V}_b$, the body force $\mathbf{f}$ must be,

$$\mathbf{f} = -RHS + \frac{\mathbf{V}_b - \mathbf{u}^n}{\Delta t} \ , \tag{2.3}$$

in the flow region where we wish to mimic the solid body and zero elsewhere. In general, the surface of the region where $\mathbf{u}^{n+1} = \mathbf{V}_b$ does not coincide with a coordinate line. In that case, the value of $\mathbf{f}$ at the node closest to the surface but outside the solid body is linearly interpolated between the value that yields $\mathbf{V}_b$ inside the solid body and the

value in the interior of the flow domain. This interpolation procedure is consistent with the centered second-order finite-difference approximation, and the overall accuracy of the scheme remains second-order (Fadlun *et al.*, (2000)).

Equations (1) have been spatially discretized in a cylindrical coordinate system using staggered central second-order finite-difference approximations. Details of the numerical method are given in Verzicco & Orlandi, (1996); only the main features are summarized here. In a three-dimensional inviscid flow without immersed boundaries and free-slip condition, kinetic energy is conserved, and this feature is retained in the spatially discretized equations.

The discretized system is integrated in time using a fractional-step method where the viscous terms are computed implicitly and the convective terms explicitly. The large sparse matrix resulting from the implicit treatment is inverted by an approximate factorization technique. At each time step the momentum equations are provisionally advanced using the pressure at the previous time step, giving an intermediate non-solenoidal velocity field. A scalar quantity Φ then is introduced to project the non-solenoidal field onto a solenoidal one. The large-band matrix associated with the elliptic equation for Φ is reduced to a penta-diagonal matrix using trigonometric expansions (FFT's) in the azimuthal direction; this matrix is inverted using the FISHPACK package (Swartzrauber, (1974)). A hybrid low-storage third-order Runge-Kutta scheme is used to advance the equations in time, and the body-forces are enforced at each stage of the Runge-Kutta scheme. It is worth noting that application of $\mathbf{f}$, in fact, does not require the computation of extra terms, but rather the cancellation of pre-existing ones. As a matter of fact, the integration of the equations with the body forces only takes 5% more CPU time than in absence of the forcing.

The simulation of the flow inside mixing devices is usually performed using RANS modeling owing to their reduced computational cost. Since one aim of the present paper is to compare the performance of DNS/LES *vs* RANS models, we have also performed a couple of RANS simulations of the flow previously described. Steady RANS equations in a frame rotating with the impeller are solved on a $1/8^{\text{th}}$ sector of the tank using a commercial CFD code. Periodicity conditions are imposed in the azimuthal direction. Low-Reynolds number turbulence models have been used, namely the $k-\epsilon$ by Launder & Sharma (1974) and the V2F model by Durbin, (1995).

3. Results

Several preliminary simulations were performed to investigate the mesh distribution and grid resolution, the necessity for a turbulence model, possible effects of the upper free-surface deformation, and how many blades of the impeller had to be simulated. Concerning the first point, grids ranging from 5×10^5 to 1.9×10^6 gridpoints have been used in order to assess the reliability and grid independence of the results.

The need for turbulence modeling has been verified by running an identical case with and without sub-grid-scale model. Given the operational conditions of the test, the Reynolds number is quite small ($Re = 1636$) and direct numerical simulation (DNS) is possible. Consistently, a simulation with the dynamic subgrid scale large eddy simulation (LES) model yielded results almost coincident with those of the DNS with a turbulent viscosity close to zero. It must be noted, however, that DNS is possible only for the present "simplified" model problem in which geometrical dimensions and rota-

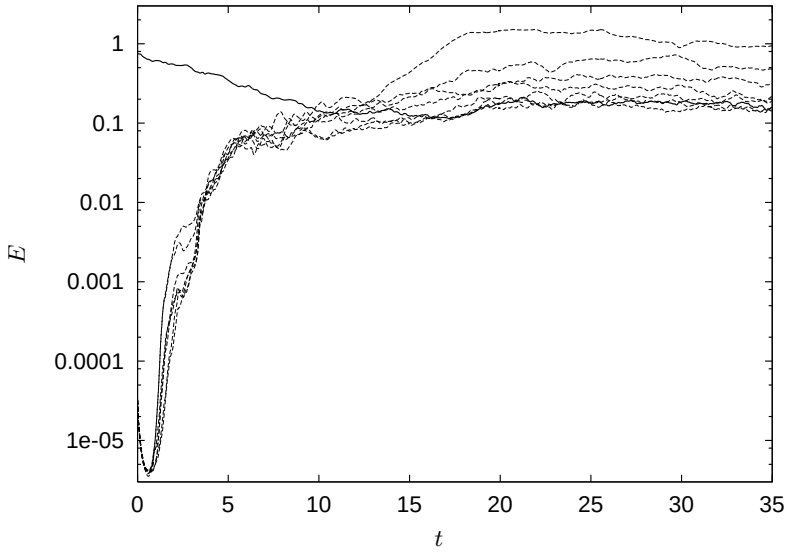

FIGURE 3. Time evolution of the kinetic energy of azimuthal modes starting from a simulation on $1/8^{\text{th}}$ of the domain and 1 impeller blade: ——— $n = 8$ mode, – – – – all modes from $n = 1$ to $n = 7$. Note that time has been rescaled so that each time unit corresponds to one rotation period of the impeller.

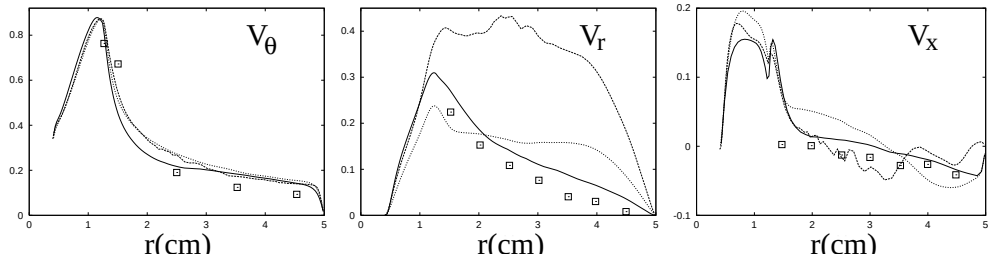

FIGURE 4. Averaged radial velocity profiles in a section crossing the impeller ($x = 4$). *Left* azimuthal velocity, *Center* radial velocity, *Right* axial velocity: – – – – simulation on $1/8^{\text{th}}$ of the domain (1 blade), ····· $1/4^{\text{th}}$ of the domain (2 blades), ——— whole domain, symbols are experimental data of Dong *et al.*, (1994).

tion speed are both small. In contrast, for the simulation of practical cases, operational conditions are more severe and the use of a turbulence model would be mandatory.

Free-surface deformation is induced by the azimuthal rotation and the resulting hydrostatic and centrifugal forces at the interface between fluid and air. This deformation is often disregarded in numerical simulations, and the upper boundary of the tank is modeled by a flat free-slip wall. This strategy was also followed in the main case presented in this report. However, a few remarks about the free-surface effects are in order. Assuming that the bulk of the flow is in solid body rotation, the shape of the free-surface would be given by $z = \Omega^2 r^2/(2g)$, which for the present flow conditions yields a maximum deformation $\Delta z \simeq 1.4$cm. This displacement is larger than the blade radius; therefore, it is in principle possible that the results would be changed by this additional effect. In one case the free-surface deformation has been modeled by the same body forces used for

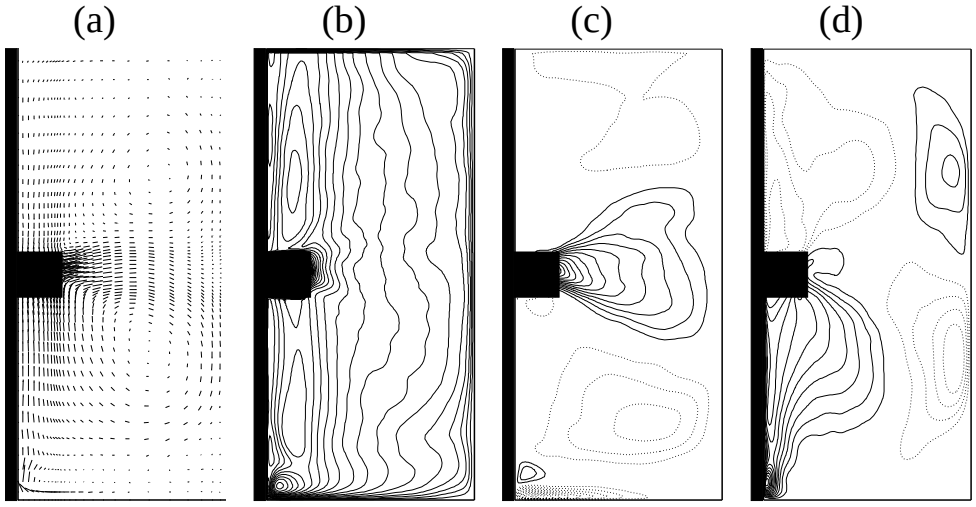

FIGURE 5. Averaged velocity fields: *(a)* velocity vector field, contours of: *(b)* azimuthal, *(c)* radial, *(d)* axial velocity components ($\Delta u = \pm 0.025$).

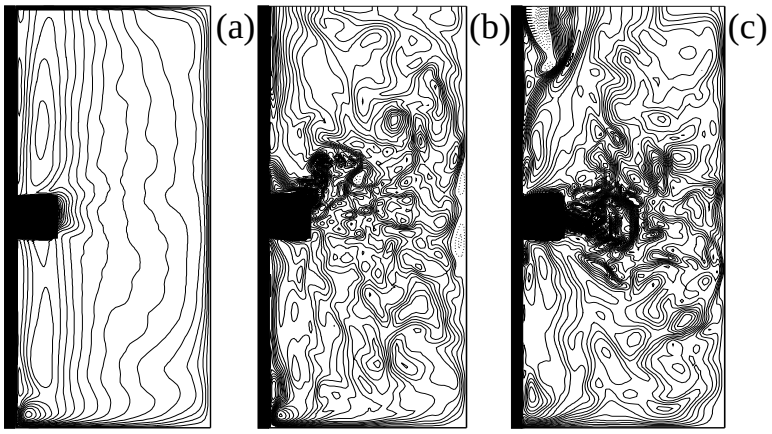

FIGURE 6. Comparison between averaged *(a)* and instantaneous *(b)*, *(c)* velocity fields: velocity magnitudes are shown, (section passing through the blade), ($\Delta u = 0.05$)

.

the rotating impeller (and therefore rotating with the same angular velocity) with the results being only slightly modified by this new effect (and only in the region close to the upper surface). We will see that, in fact, the flow rotates much slower than a solid-body rotation; therefore, the free-surface deformation would be smaller than previously estimated. This implies that the approximation of the upper surface as a flat, stress-free boundary is indeed appropriate.

Since the impeller consists of 8 equispaced blades, it is tempting, for computational purposes, to reduce the domain to $1/8^{\text{th}}$ of the tank and only one blade; this assumption yields a considerable reduction of computational effort. Nevertheless, it must be noted that on a domain reduced to $1/8^{\text{th}}$ of the azimuthal span, only structures with 8-fold symmetry and multiples can be supported. This prevents the development of modes smaller than 8 and of all the modes which are not multiples of 8. We have verified by

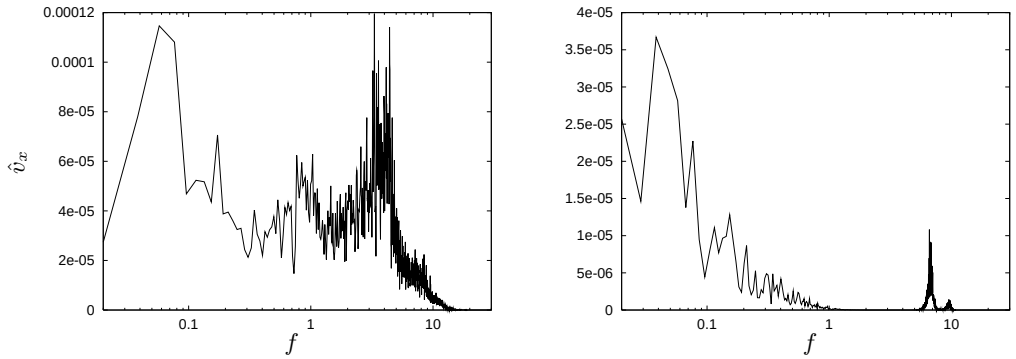

FIGURE 7. Frequency spectra of the axial velocity component for the probes at $(r = 2, x = 4)$ (Left) and $(r = 2, x = 2)$ (Right). The probes are, respectively, in the radial jet emanating from the impeller and in the center of the lower meridional recirculation. Note that the frequencies in the abscissa have been rescaled so that $f = 1$ corresponds to the rotation period of the impeller.

simulations which included one or two impeller blades, and therefore on $1/8^{\text{th}}$ and $1/4^{\text{th}}$ of the domain, respectively, that this assumption is not appropriate for the present problem and that the results were significantly different from the experiments. The inadequacy of the simulation on $1/8^{\text{th}}$ of the domain is confirmed also by Fig. 3 showing the time evolution of the azimuthal energy modes for a simulation over the whole domain but initiated from a simulation performed over a $1/8^{\text{th}}$ sector. We can see that the energy in the $n = 8$ mode slowly decreases in time while the lower modes experience an exponential growth and after saturation attain an energy comparable or bigger than the original mode. This shows that the 8-fold symmetry was only an artifact of the computational domain while the system would tend to distribute the energy also among odd and low-order modes. This point is further stressed by the velocity profiles shown in Fig. 4 where it is shown that the radial velocity is severely overpredicted in the simulation over $1/8^{\text{th}}$ of the domain. This overprediction is less evident when the simulation is extended over two impeller blades while the best results are obtained for the whole domain. It is worth mentioning that the prediction of the azimuthal velocity profiles is as accurate as in Fig. 4 for all the radial sections, and it is independent of whether a section or the whole domain is simulated. Radial and axial velocity profiles, in contrast, are much more sensitive to the azimuthal extension of the domain, and this point will be further discussed when comparing the DNS with RANS results. From the above results it is concluded that, in order to get accurate simulations, it is not possible to reduce the domain using impeller symmetries, but the whole problem must be solved.

We shall now describe the results of the DNS simulation simulation and compare it with the available experimental and RANS data. In Fig. 5 we report the computed mean field, averages being performed in the azimuthal direction and in time.

It is evident that the meridional plane is roughly divided into two halves by the radial jet emanating from the impeller. It can be noted, however, that the two recirculations are not symmetric owing to the different boundary conditions on the upper and lower horizontal surfaces. An important effect of the lower no-slip wall is the strongly positive vertical velocity in the lower half of the domain in the region close to the shaft (Fig. 5d). This effect is characteristic of wall-bounded rotating flows and is known as 'Eckman-pumping'; it causes the fluid to be pushed radially inward at the plate (Fig. 5c) and

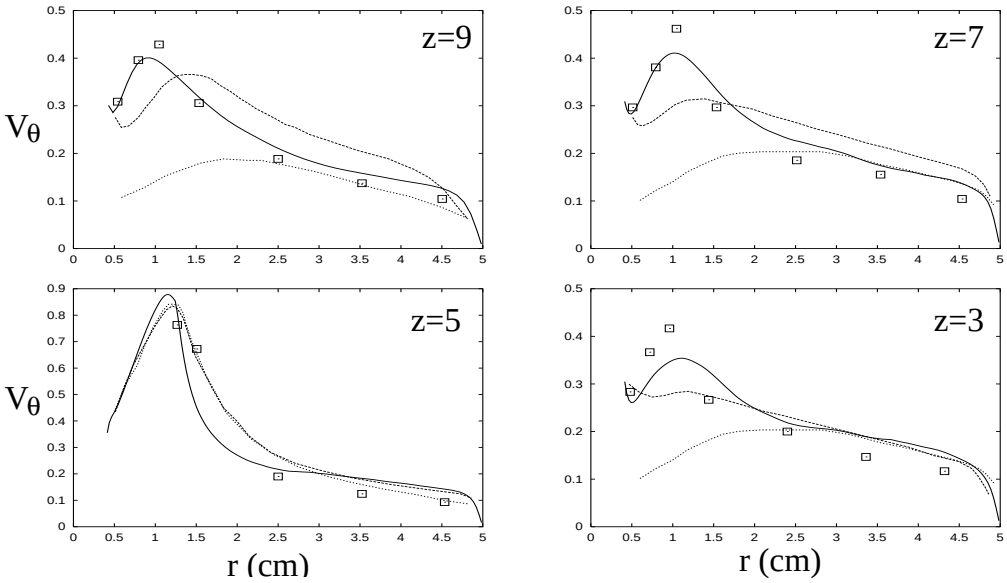

FIGURE 8. Radial profiles of averaged azimuthal velocity at different heights in the tank: ——— present DNS results, – – – – RANS simulation with the V2F model, ····· RANS simulation with $k-\epsilon$ model, Symbols are experiment by Dong *et al.* (1994). The radial coordinate is in centimeters and the azimuthal velocity is scaled by the blade tip velocity. (The values of z are in tenth of the tank height).

axially upward at the axis of rotation (Fig. 5d). Because of mass conservation, a vertical ascending fluid column at the axis induces a descending current at the external radial wall, thus reinforcing the lower-half recirculation with respect to the upper one. This is also well evidenced by the radial jet that does not point exactly in the radial direction, but rather has a positive vertical velocity close to the blade region and then a weakly negative vertical velocity.

In Fig. 6 instantaneous snapshots analogous to those of Fig. 5 are reported and compared with an averaged field, thus confirming the strongly unsteady nature of the flow. This point is further stressed by the analysis of the velocity signals taken from the numerical probes whose positions are reported in Fig. 2. Spectra are computed from the temporal series and are plotted in semi-log axes in order to separate the frequency peaks due to coherent motion from the background turbulence (Fig. 7). It can be noticed that many widely separated frequencies are present, and these range from the slow dynamics due to the precession and meridional oscillation of the large-scale recirculation to the fast vortex shedding at the blade tips†. Given the different time-scales of the described flow phenomena, it is very difficult for the RANS models to correctly parameterize all of the flow fluctuations, and this is confirmed by the velocity profile results.

Radial profiles of azimuthal, radial, and vertical velocity components are compared with experimental data and RANS simulations in Figs. 8, 9, and 10. The DNS prediction for the azimuthal velocity component is quite accurate, in particular in the region near the shaft above and below the impeller where a peak is observed. This is due to the large

† Note that in the spectra, the peak corresponding to the period of revolution of the impeller is missing because the equations are solved in a frame of reference rotating with the blade.

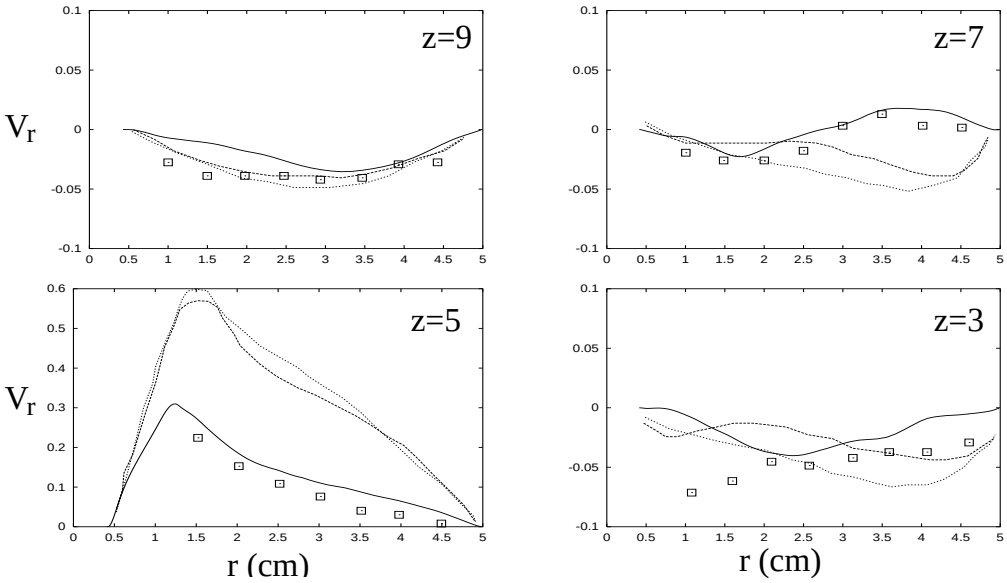

FIGURE 9. The same as Fig. 8 for averaged radial velocity.

scale recirculation that drives the fluid from the external radial region towards the axis, thus increasing the azimuthal velocity owing to the conservation of angular momentum. Except for the section crossing the impeller, RANS simulations severely underpredict the peak velocity, thus confirming the findings of Jones, *et al.*, (2000). As already mentioned, the accurate DNS prediction of the azimuthal velocity profiles is independent of the computational domain extension; therefore, the RANS velocity underprediction must be attributed to the inadequacy of the modeling for this flow and not to the restriction of the computational domain to $1/8^{\text{th}}$ of the full size.

Radial and vertical velocity components are also accurately predicted by the DNS simulation with results that are generally better than RANS. This is especially true for the radial velocity profile in the section crossing the blade where RANS results overpredicted the velocity by more than a factor of two. This mismatch, however, can only partially be attributed to RANS modeling since a major effect is induced by the limitation of the computational domain to only one blade as shown in Fig. 4.

4. Conclusions

In this paper we have performed a DNS of flow in an impeller stirred unbaffled cylindrical tank with an immersed boundary procedure to deal with the complex geometry. The main motivation comes from the literature showing that, although the geometry is relatively simple and the Reynolds number quite low, standard RANS simulations yield a very poor flow prediction.

It is found that the flow is strongly unsteady and inhomogeneous even if the Reynolds number is low enough to make the DNS affordable. Accordingly, an LES simulation with a dynamic subgrid-scale model yielded the same results as the DNS with a turbulent viscosity close to zero. RANS models, in contrast, can not automatically switch off when the

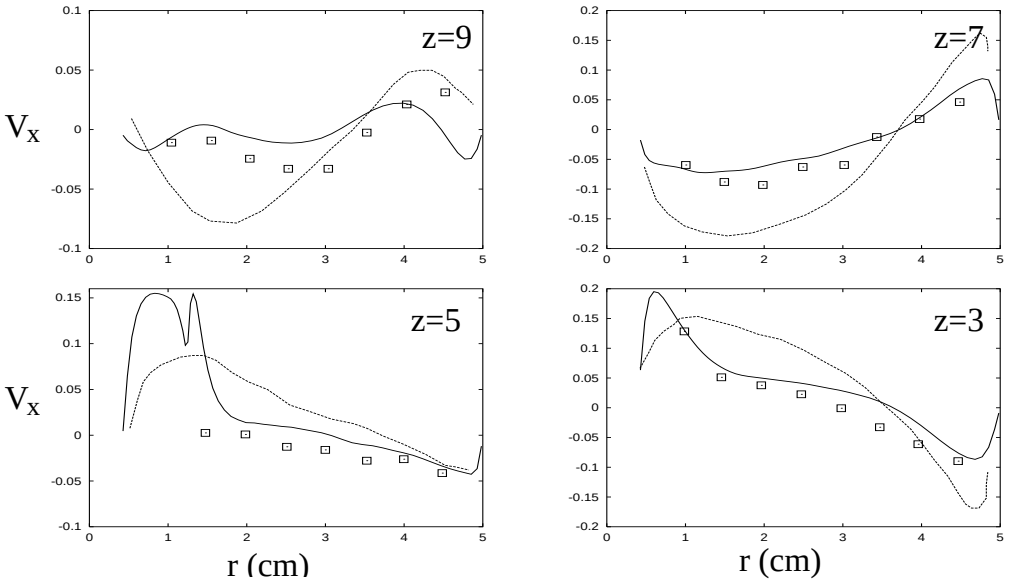

FIGURE 10. The same as Fig. 8 for averaged axial velocity. ($k-\epsilon$ RANS data are missing).

resolution is fine enough, and they parameterize all the velocity oscillations as turbulent fluctuations.

Since the impeller has 8 azimuthally equispaced blades, simulations in the literature have always been performed over a sector of the domain spanning $1/8^{\text{th}}$ of the domain. Although this assumption reduces the computational cost by a factor of 8, the results do not agree with the experiments since the flow is forced to maintain a symmetry that is not physical. A posteriori this result is not surprising since, looking at Fig. 1, it is unlikely that blades whose area is less than $1/50^{\text{th}}$ of the meridional section could enforce any symmetry on the large-scale flow.

Some remarks of the computational costs of these DNS simulations are in order. In contrast to RANS where a steady solution is forced, for unsteady simulations mean quantities are obtained by averaging the solution in time. In the present case, the intense velocity fluctuations required long-term averages (typically 15-20 impeller revolutions) to obtain smooth converged statistics. This must be added to the initial transient that consisted of an equivalent time of about 40 impeller revolutions on the finest grid. The computation of this flow evolution is highly expensive compared to RANS simulations where the mean field is directly obtained. Fortunately, the use of the immersed boundary procedure makes the simulation of complex-geometry three-dimensional unsteady flows quite affordable. As an example, in the present case on a grid of 1.9×10^6 points, the code uses 85Mb of RAM and requires 32s for each 3^{rd} Runge-Kutta time step (consisting of three complete substeps) on a single 900MHz Athlon processor; the entire simulation required slightly less than 5 days.

REFERENCES

DONG, L., JOHANSEN, S. T. & ENGH, T. A. 1994 Flow Induced by an Impeller in an Unbaffled Tank-I. Experimental. *Chem. Engng. Sci.* **49**(4), 549.

Durbin, P. A. 1995 Separated Flow Computations with the $k-\epsilon-v^2$ Model. *AIAA J.* **33**, 659.

Fadlun, E. A., Verzicco, R., Orlandi, P. & Mohd-Yusof, J. 2000 Combined immersed-boundary/finite-difference methods for three-dimensional complex flow simulations. *J. of Comp. Phys.* **161**, 35.

Jones, R. M., Harvey III, A. D. & Acharya, S. Two-Equation Turbulence Modeling for Impeller Stirred Tanks. *Private communication*.

Launder, B. E., & Sharma, A. 1974 Application of the Energy-Dissipation Model of Turbulence to the Calculation of Flow Near a Spinning Disk. *Letters in Heat and Mass Transfer*. **1**, 131.

Swartzrauber, P. N. 1974 Direct Method for the Discrete Solution of Separable Elliptic Equations. *SIAM J. Num. Anal.* **11**, 1136.

Verzicco, R. & Orlandi, P. 1996 A finite-difference scheme for three-dimensional incompressible flows in cylindrical coordinates. *J. of Comp. Phys.* **123**, 402.

Verzicco, R., Mohd-Yusof, J., Orlandi, P. & Haworth, D. 2000 Large Eddy Simulation in Complex Geometric Configurations Using Boundary Body Forces. *AIAA J.* **38**(3), 427.